Bond of nanoinclusions reinforced concrete with old concrete: strength, reinforcing mechanisms and prediction model

Xinyue Wang[1], Sufen Dong[2,*], Ashraf Ashour[3], Baoguo Han[1,*]

[1]*School of Civil Engineering, Dalian University of Technology, Dalian, 116024 China*
[2]*School of Material Science and Engineering, Dalian University of Technology, Dalian, 116024 China*
[3]*Faculty of Engineering & Informatics, University of Bradford, Bradford, BD7 1DP, UK*
* Corresponding author: hithanbaoguo@163.com, dongsufen@dlut.edu.cn

Abstract:

This paper investigated the bond strength of eight nanoinclusions reinforced concrete with old concrete through a splitting tensile test. The reinforcing mechanisms of bond due to nanoinclusion was also explored by means of scanning electron microscope and energy dispersive spectrometer. A prediction model for the bond strength between nanoinclusion reinforced concrete with old concrete substrate was developed and calibrated against the experimental results obtained. The experimental results indicated that bond strength between nanoinclusions reinforced concrete and old concrete can reach 2.85 MPa, which is 0.8 MPa/39.0% higher than that between new concrete without nanoinclusions and old concrete. The reinforcing mechanisms can be attributed to the enrichment of nanoinclusions in the new-to-old concrete interface, compacting the interfacial microstructures and connecting hydration products in micropores of old concrete with that in bulk new concrete. In addition, the prediction model proposed on the basis of reinforcing mechanisms can accurately describe the relationship of the nanoinclusion content and the bond strength of nanoinclusions reinforced concrete with old concrete.

Keywords: Nanoinclusions reinforced concrete; New-to-old concrete; Bond strength; Reinforcing mechanisms; Prediction model

1 Introduction

A large number of concrete structures cannot reach their design service life due to damage caused by the combined effects of mechanical loads and environmental factors, for example fatigue, shrinkage, creep, temperature change, freeze-thaw weathering, etc. In order to prolong the service life of deteriorated concrete structures, repair and rehabilitation using new concrete is generally adopted. However, it is estimated that about half of concrete repairs fail; most of which can be attributed to debonding at the new-to-old concrete interfaces, confirming the importance of reliable bonding between new and old concretes [1-3].

Bond strength is a key indicator, representing the quality of interface between new and old concretes. Such new-to-old concrete bond strength is mainly governed by mechanical interlock and van der Waals forces, which is influenced by interface roughness (affecting mechanical interlock), the shrinkage difference of new and old concrete (affecting interfacial internal stress state), the microstructures of the new-to-old concrete interface (affecting van der Waals forces), etc. [4, 5]. Based on the factors governing the bond strength between new and old concretes, previous research investigations have taken two directions to improve such bond strength. The first one is focused on preparation techniques to increase the surface roughness of old concrete, therefore, dramatically enhancing the mechanical interlock between new and old concretes. It is reported that the bond strength between new and old concretes with rough surface is several to over ten times higher than that with smooth surface [6-8]. However, this method is difficult to be applied in repairs of inherent structural cracks. The second technique is mainly concerned with the development of improved repair materials that are volumetrically stable, i.e. undergo neither shrinkage nor expansion once installed, and would display compatible modulus of elasticity, strength, creep, shrinkage, thermal expansion, permeability and electrochemical characteristics to the substrate existing concrete. For example, fibers, mineral additives, and shrinkage reducing agents are incorporated so as to limit the shrinkage difference between new and old concrete [9-12]. Meanwhile, nanoinclusions have been certificated to be effective in improving the mechanical properties and durability of concrete, through densifying microstructures and reducing shrinkage of concrete [13-19]. This is beneficial to achieve reliable bonding between nanoinclusions reinforced concrete and old concrete, showing a promising material for concrete rehabilitation and strengthening [20-26]. The observed best modification of bond strength between nanoinclusions reinforced concrete and old concrete with smooth surface includes a 29.5% increase in tensile strength [21] and a 21.6% increase in slant shear strength [22]. However, there is a lack of broader research with regard to the quantification of bond strength between different types of nanoinclusions reinforced concrete and old concrete, a better understanding of reinforcing mechanisms to further control the repair effects of nanoinclusions reinforced concrete and development of prediction models of bond strength between nanoinclusions reinforced and old concretes.

Therefore, this paper aims to investigate the bond strength, reinforcing mechanisms and prediction model of nanoinclusions reinforced concrete with old concrete. A splitting tensile test was carried out to determine the bond strength between eight different types of nanoinclusions reinforced concrete and old concrete as well as the splitting tensile strength of concrete with nanoinclusions. After the splitting tensile test, scanning electron microscope (SEM) and energy dispersive spectrometer (EDS) were performed in order to explore the reinforcing mechanisms. Finally, a prediction model of bond strength between nanoinclusions reinforced concrete and old concrete was established.

2 Experimental programs

2.1 Materials and mix design

Due to their small size, nanoinclusions can only affect concrete in a small range around them, but cannot fill the larger pores [27, 28]. Concrete with compact microstructure may fully achieve the reinforcing effect of nanoinclusions. Therefore, reactive powder concrete was selected in this study where the modified Andreasen and Andersen packing model [29] is used for mix design of concrete, as presented by Formula 1 below.

$$P(D) = \frac{D^q - D_{min}^q}{D_{max}^q - D_{min}^q} \quad (1)$$

where D is the particle size of solid particles in concrete; D_{max} and D_{min} are the maximum and minimum particle size; q is the distribution modulus ranging from 0 to 0.28 according to the previous researches [30-32], and its value in this study is equal to 0.28; $P(D)$ is the fraction of the total solid particles being smaller than D.

Ordinary Portland cement with a strength of 42.5 R is employed for all specimens prepared in this study. Quartz sand with a size range of 0.12-0.83 mm is used as aggregate. The polycarboxylate superplasticizer has a reducing water capability to an extent of 30%. In addition, class II fly ash and silica fume with the average particle size of 0.15 μm are used as mineral mixtures in this study. Eight different types of nanoinclusions are selected to reinforce the new concrete according to previous studies [33]; the properties of which are listed in Table 1. The contents of different nanoinclusions are determined on the basis of the previous literature [33]. The mix proportions of concrete with different types of nanoinclusions are listed in Table 2.

Table 1. Properties of nanoinclusions

Types	Abbreviation	Purity (%)	Diameter (nm)	Length (μm)	Thickness (nm)	Density (g/cm^3)	Specific surface area

							(m^2/g)
Nano silica	S	≥99	20	-	-	2.2	≥600
Silica-coated rutile titania	T	≥96	20	-	-	4	-
Monoclinic zircon	Z	≥99	20	-	-	5.8	≥25
CNTs	CNTs	-	20-30	0.5-2	-	2.1	>120
Hydroxyl functionalized CNTs	H-CNTs	-	<8	0.5-2	-	2.1	>380
Nickel coated CNTs	Ni@CNTs	-	20-30	10-30	-	6.2	70
Multi-layer graphene	MLG	-	<2000	-	1-5	2.25	500
Nano BN	NB	99.9	120	-	5-100	2.3	19

Table 2 The mix proportions of nanoinclusions reinforced concrete

Nanoinclusion	Code	Mix proportions (mass ratio)						
		Cement	Nanofillers	Fly ash	Silica fume	Aggregate	Water	Superplasticizer (%)
Control mix	Blank*	1	-	0.25	0.313	1.375	0.375	1.5
	S-1	0.99	0.01					2.0
S	S-2	0.98	0.02	0.25	0.313	1.375	0.375	2.5
	S-3	0.97	0.03					3.0
	T-1	0.99	0.01					
T	T-2	0.98	0.02	0.25	0.313	1.375	0.375	1.5
	T-3	0.97	0.03					
	Z-1	0.99	0.01					
Z	Z-2	0.98	0.02	0.25	0.313	1.375	0.375	1.5
	Z-3	0.97	0.03					
	CNTs-0.1	0.999	0.001					
CNTs	CNTs-0.3	0.997	0.003	0.25	0.313	1.375	0.375	1.5
	CNTs-0.5	0.995	0.005					
	H-CNTs-0.1	0.999	0.001					
H-CNTs	H-CNTs-0.3	0.997	0.003	0.25	0.313	1.375	0.375	1.5
	H-CNTs-0.5	0.995	0.005					
	Ni@CNTs-0.1	0.999	0.001					
Ni@CNTs	Ni@CNTs-0.3	0.997	0.003	0.25	0.313	1.375	0.375	1.5
	Ni@CNTs-0.5	0.995	0.005					
	MLG-0.1	0.999	0.001					
MLG	MLG-0.3	0.997	0.003	0.25	0.313	1.375	0.375	1.5
	MLG-0.5	0.995	0.005					
	NB-0.1	0.999	0.001					
NB	NB-0.3	0.997	0.003	0.25	0.313	1.375	0.375	1.5
	NB-0.5	0.995	0.005					

* Blank is used for the old concrete and the new concrete without nanoinclusions.

2.2 Specimen preparation

In this study, specimens with scale-up interface were fabricated, the geometric dimension of which is exhibited in Figure 1 (a). The concrete blocks with size of 40 mm×40 mm×80 mm were, initially, cured in water for 28d and, then, in air for 365d.

These concrete blocks were used as old concrete to fabricate the specimens with new-to-old concrete interface. The key issue in specimen preparation is to homogeneously disperse nanofillers in RPC [34, 35]. Poor dispersion of nanofillers weakens the nanofiller modification effect or even acts as defects in concrete. This study used polycarboxylate superplasticizer as dispersing agent. Additionally, stirring and ultrasonic were applied for dispersing non-carbon nanofillers (namely nano silica, nano titania, nano zircon, and nano BN) and carbon nanofillers (namely CNTs, H-CNTs, Ni@CNTs, and multi-layer graphene). Using these dispersing methods, different nanofillers can be evenly distributed in concrete matrix [36, 37]. The detailed fabrication process of specimens refers to previous examples from the literature [33].

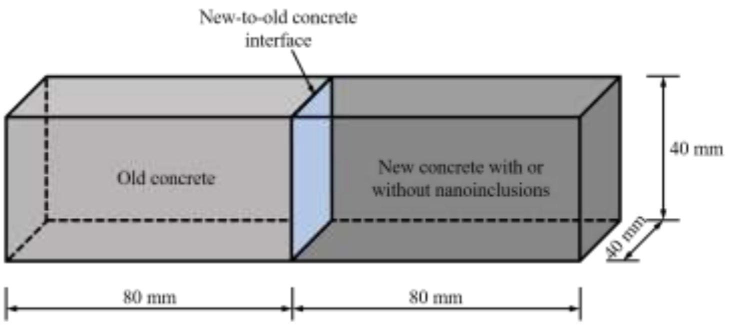

(a) The geometric dimension of specimens.

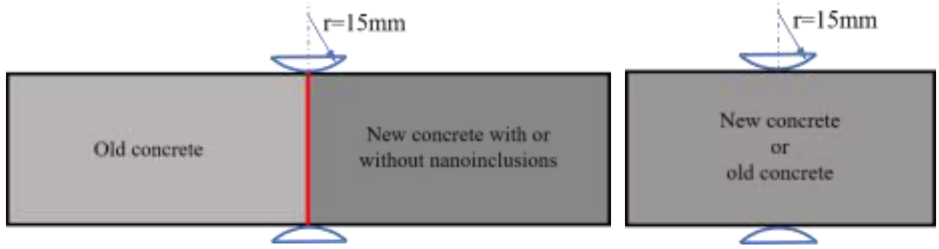

(b) The splitting tensile test

Figure 1. Experimental diagrams

2.3 Measurements

According to Chinese National Standard GB/T 50081-2019 [38], the splitting tensile test was performed on six specimens in each group to evaluate the bond strength of nanoinclusions reinforced concrete with old concrete, as shown in Figure 1 (b). The average value of the bond strengths of 6 specimens in each group was recorded as the final bond strength. The test specimens were loaded to failure at a displacement control rate of 0.02 mm/min. The splitting tensile strength f_t is calculated by Formula 2 [38].

$$f_t = \frac{2P}{\pi A} \tag{2}$$

where P is the maximum applied load, and A (=1600 mm^2) is the area of the bonding plane. In addition, the splitting tensile test was also performed on old concrete or nanoinclusions reinforced concrete to characterize the splitting tensile strength for each material alone, as shown in Figure 1 (b).

After the splitting tensile test, SEM and EDS were performed to observe the microstructure and morphology of the hydration products on the two failure surfaces (old concrete side and nanoinclusions reinforced concrete side) of each group. Moreover, the EDS mapping analysis was carried out on titanium, zirconium, and nitrogen that are different from the components of cement and the elements introduced in sample pretreatment.

3 Results and discussions

3.1 Bond strength

In this experiment, all specimens were failed along the interface between nanoinclusions reinforced concrete and old concrete, as shown in Figure 2. Therefore, the bond strength can be calculated by Formula 2. Figure 3 demonstrates the bond strength between new concrete with/without nanoinclusions and old concrete, indicating that the bond strength of nanoinclusions reinforced concrete with old concrete is higher than that of new concrete without nanoinclusions with old concrete. For nanoparticles, the bond strengths of specimens with 1 wt.% of S, 3 wt.% of T, and 2 wt.% of Z are 2.38 MPa, 2.62 MPa, and 2.43 MPa, respectively; while that of the specimen without nanoinclusions is 2.05 MPa. As for nanotubes, the incorporation of 0.3 wt.% of CNTs, 0.3 wt.% of H-CNTs, and 0.5 wt.% of Ni@CNTs in the new concrete makes the bond strength reach 2.54 MPa, 2.57 MPa, and 2.76 MPa, respectively. Similarly, when 0.5 wt.% of MLG and 0.5 wt.% of NB are added to the new concrete, the bond strengths reach the maximum value of 2.85 MPa and 2.76 MPa. By comparison, bond strengths of nanoinclusions reinforced concrete and old concrete in this study are superior to previous research [21-24].

Figure 2. Representative failure form

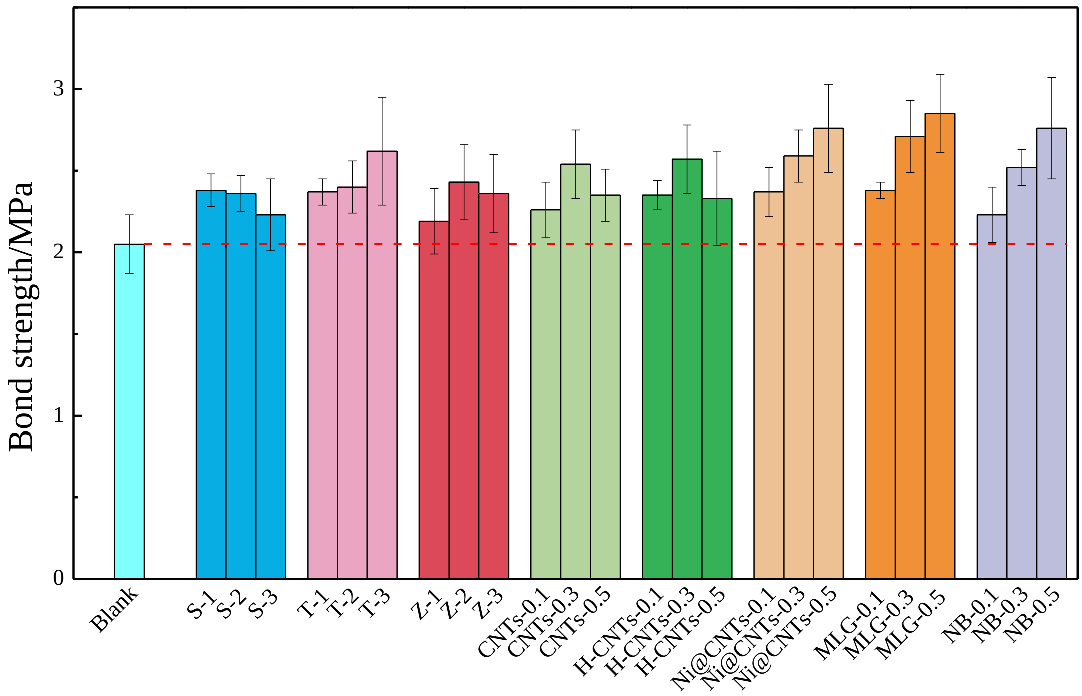

Figure 3. The bond strength between new concrete with/without nanoinclusions and old concrete

Figure 4 illustrates the splitting tensile strength of new concrete with/without nanoinclusions and old concrete. The experimental results show that the splitting tensile strength of concrete can be enhanced by adding nanoinclusions. In addition, the splitting tensile strength increases with the contents of nanoinclusions. Comparing with concrete without nanoinclusions, the splitting tensile strengths of concrete achieve the highest relative/absolute increases of 1.59 MPa/45.2%, 1.32 MPa/37.5%, and 1.26 MPa/35.8% when 3 wt.% of S, T, and Z are added respectively. As for nanotubes, concrete with 0.5 wt.% H-CNTs shows the highest splitting strength, achieving an increase of 1.84 MPa/52.3%. Meanwhile, the presence of 0.5 wt.% of CNTs and Ni@CNTs can maximally increase the splitting strength of concrete by 1.65 MPa/46.9% and 1.41 MPa/40.1%, respectively. In addition, concrete with 3 wt.% of MLG and NB shows the greatest increase of 1.60 MPa/45.5% and 1.20 MPa/34.1% in splitting strength. The splitting strength of old concrete is 0.57 MPa/16.2% higher than the new concrete without nanoinclusions due to strength development after 28d.

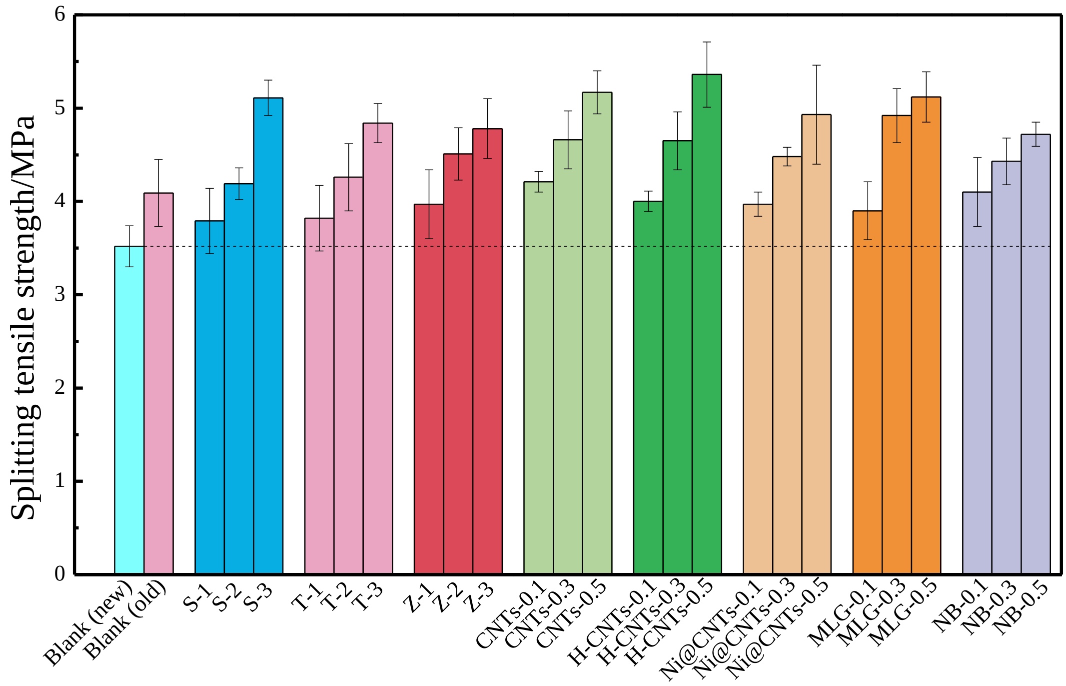

Figure 4. The splitting tensile strength of new concrete without/with nanoinclusions and old

concrete

3.2 Reinforcing mechanisms for bond strength

The reinforcing mechanisms for bond strength of nanoinclusions reinforced concrete with old concrete are revealed by SEM observations and EDS analyses. In this study, EDS mapping analysis is performed on the interior and interface of the nanoinclusions reinforced concrete in order to characterize the distribution of nanoinclusions in concrete. For this purpose, the images are firstly converted into gray-scale images, and the average gray value is calculated [39]. It can be deduced that the average gray value of the EDS mapping image is larger when there are more nanoinclusions in the analysis area. The calculated average gray value of concrete interior with 3 wt.% of T is 1.02, while that of concrete interface is 2.12, indicating that the quantity of T in new-to-old concrete interface is about 2.08 times larger than that in the nanoinclusions reinforced concrete interior. Similarly, the quantity of Z and NB in the new-to-old concrete interface are 1.47 and 1.37 times larger than that in the concrete interior, respectively.

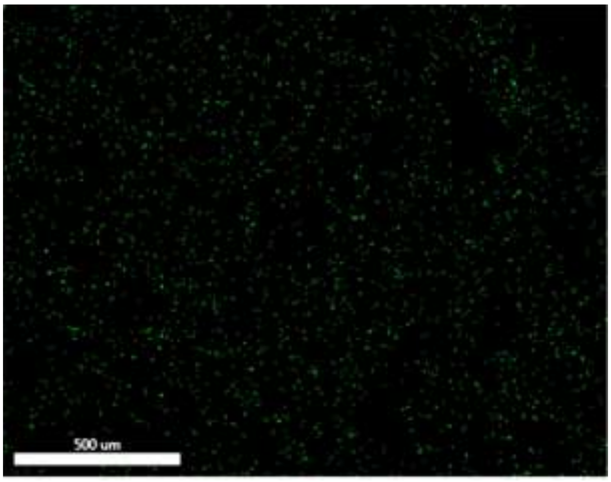

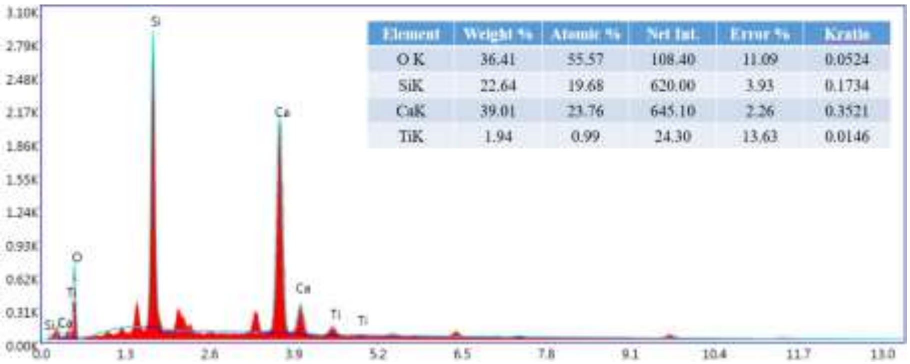

Element	Weight %	Atomic %	Net Int.	Error %	Kratio
O K	36.41	55.57	108.40	11.09	0.0524
SiK	22.64	19.68	620.00	3.93	0.1734
CaK	39.01	23.76	645.10	2.26	0.3521
TiK	1.94	0.99	24.30	13.63	0.0146

(a) Distribution of titanium in the new-to-old concrete interface

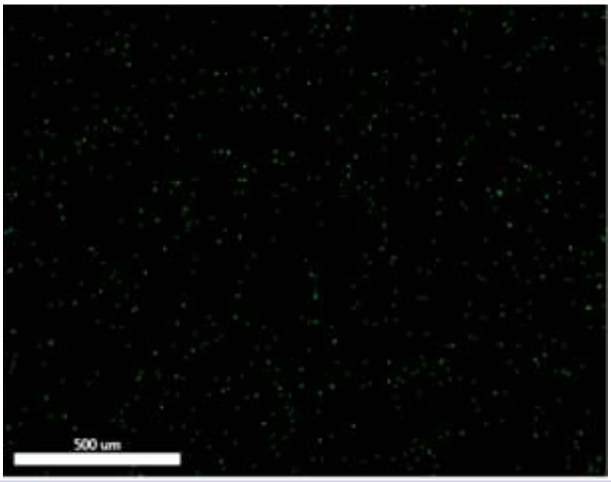

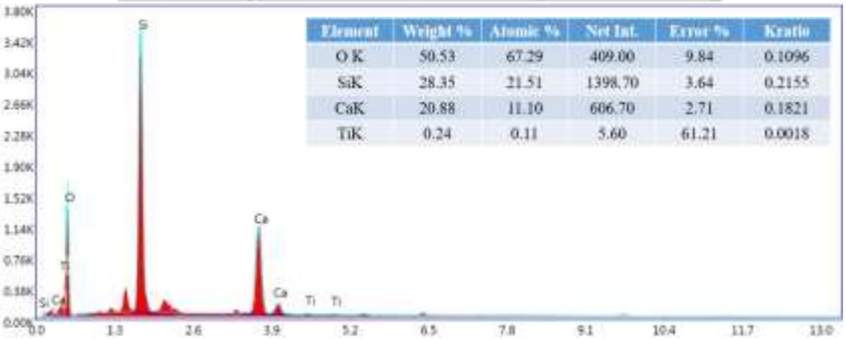

Element	Weight %	Atomic %	Net Int.	Error %	Kratio
O K	50.53	67.29	409.00	9.84	0.1096
SiK	28.35	21.51	1398.70	3.64	0.2155
CaK	20.88	11.10	606.70	2.71	0.1821
TiK	0.24	0.11	5.60	61.21	0.0018

(b) Distribution of titanium in the new concrete interior

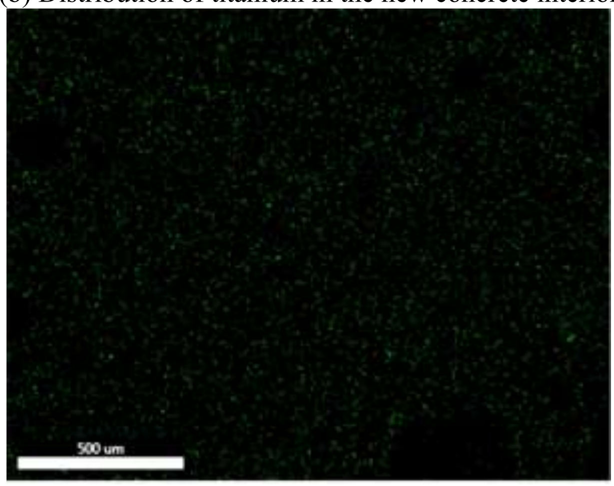

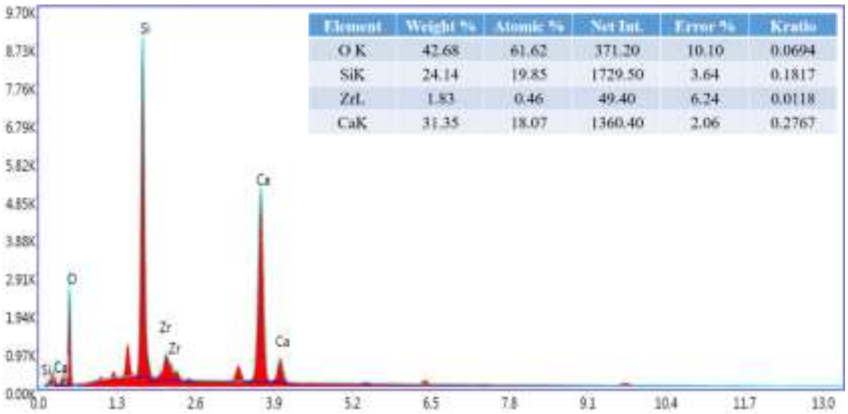

(c) Distribution of zirconium in the new-to-old concrete interface

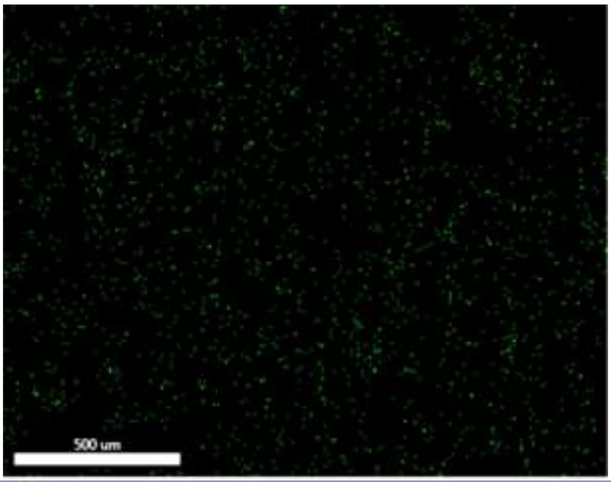

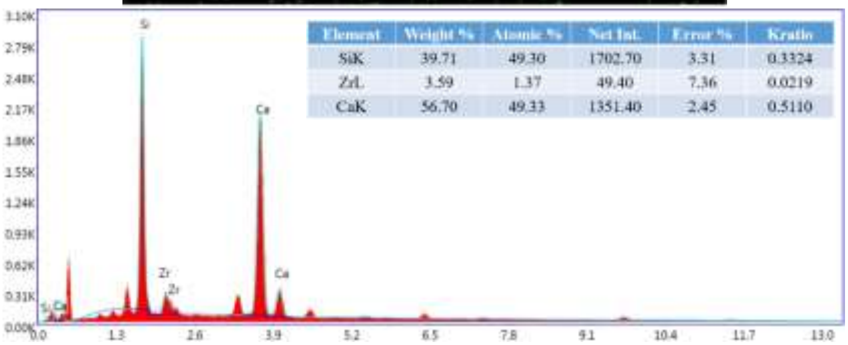

(d) Distribution of zirconium in the new concrete interior

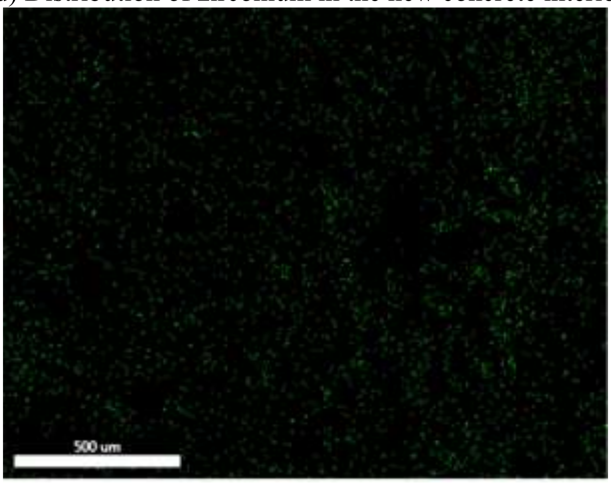

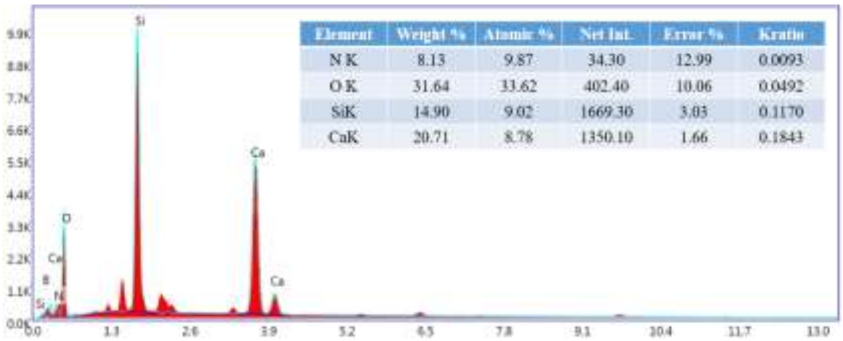

(e) Distribution of nitrogen in the new-to-old concrete interface

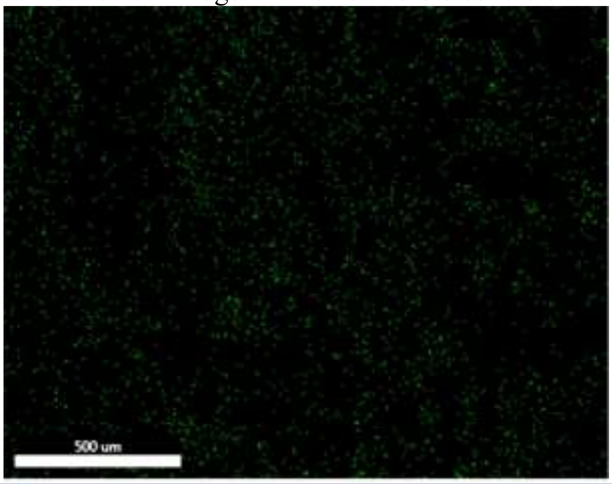

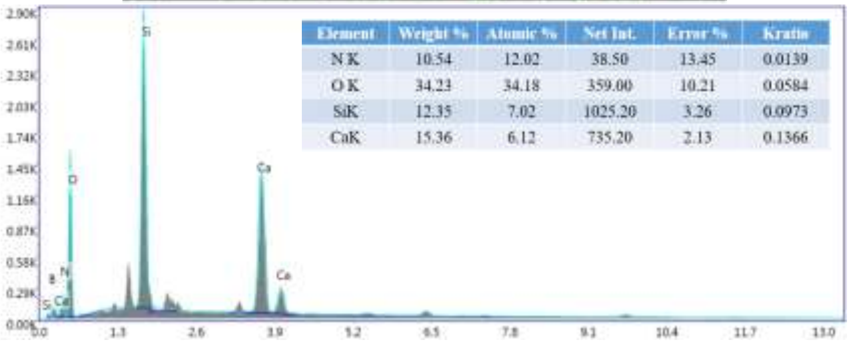

(f) Distribution of nitrogen in the new concrete interior

Figure 4. The results of EDS mapping analyses on the new concrete with 3 wt.% of T, 2 wt.% of Z, and 0.5 wt.% of NB as well as the new-to-old concrete interface

The EDS mapping results show that nanoinclusions enrich in the new-to-old concrete interface as explained by the wall effect and nanoinclusion migration effect, as shown in Figure 6. The smaller particles in fresh concrete firstly transfer toward old concrete surface while the larger particles move away from old concrete surface due to the wall effect, resulting in the phenomenon called scale separation. Afterwards, water is absorbed by old concrete and migrates toward the old concrete surface, causing nanoinclusions migrating with water in the voids among non-nano particles, and finally forming a nanoinclusion enrichment layer in the new-to-old concrete interface.

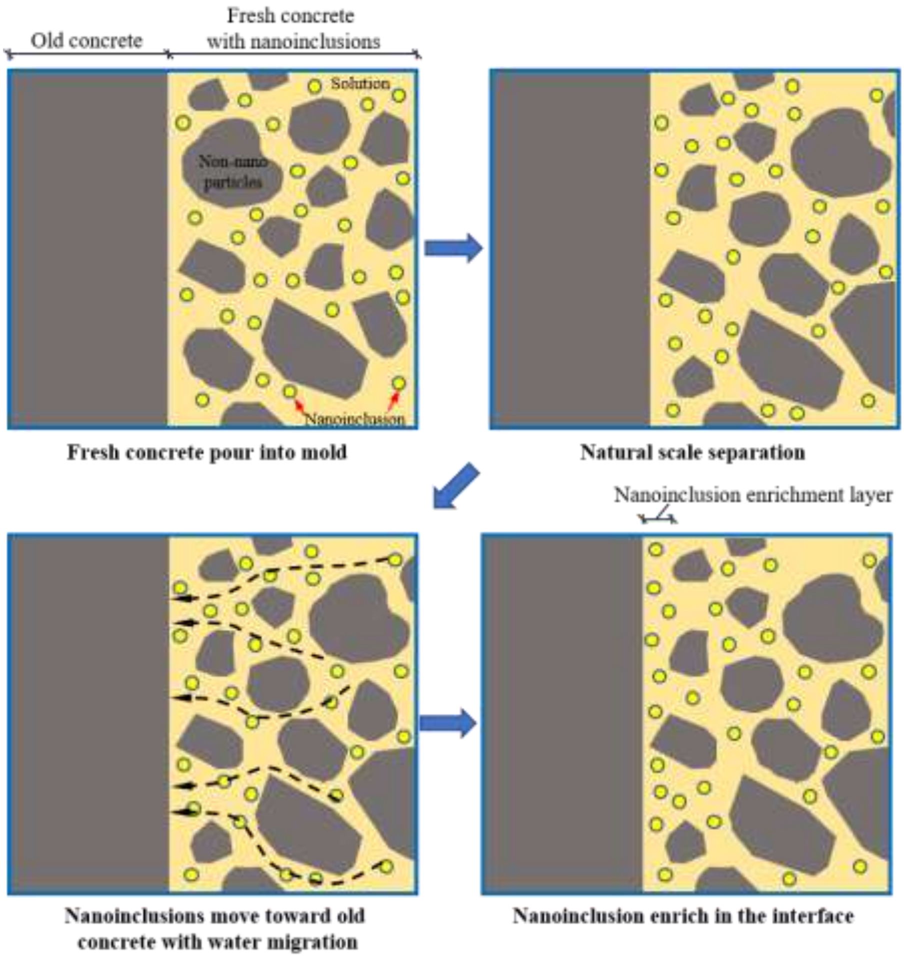

Figure 6. The formation process of nanoinclusion enrichment layer in the new-to-old concrete interface (non-nano particles include aggregates, cement particles, fly ash particles and silica fume particles)

Figure 7 exhibits the original microstructures of the hydration products on the fracture surfaces of nanoinclusions reinforced concrete. It is observed that a large amount of oriented calcium hydroxide (CH) crystal appears on the fracture surface of new concrete without nanoinclusions. In contrast, the microstructures of new concrete with 3 wt.% of T, 1 wt.% of S, 0.5 wt.% of Ni@CNTs, 0.5 wt.% of MLG, and 0.5 wt.% of NB are more compact, showing no obvious CH crystal.

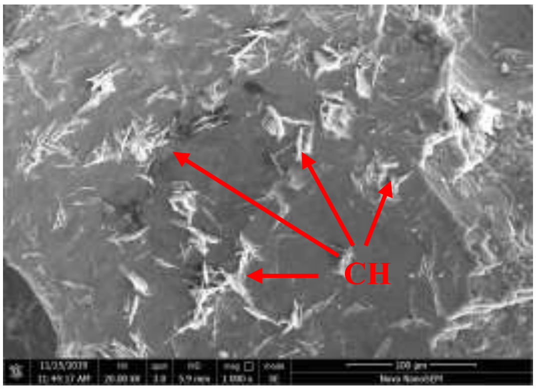

(a) Microstructures of the hydration products on the fracture surface of new concrete without nanoinclusions (1000×)

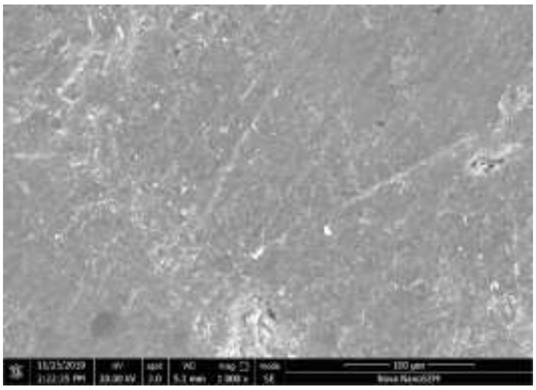

(b) Microstructures of the hydration products on the fracture surface of new concrete with 3 wt.% of T (1000×)

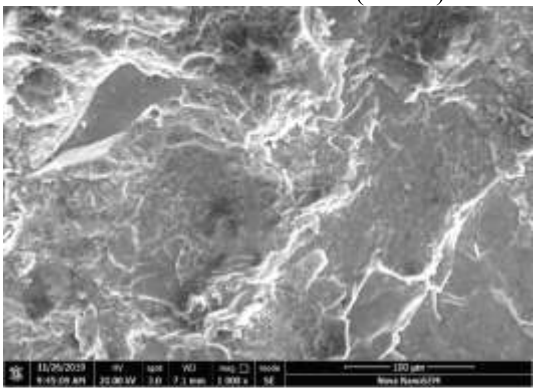

(c) Microstructures of the hydration products on the fracture surface of new concrete with 1 wt.% of S (1000×)

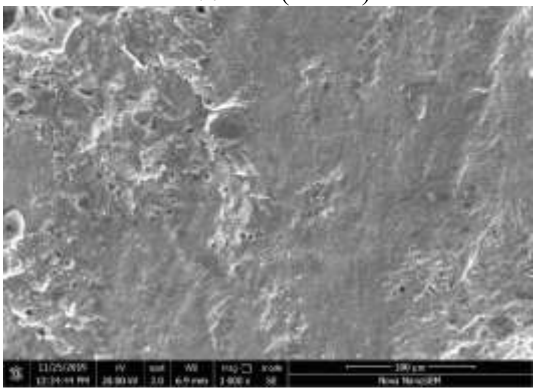

(d) Microstructures of the hydration products on the fracture surface of new concrete with 0.5 wt.% of Ni@CNTs (1000×)

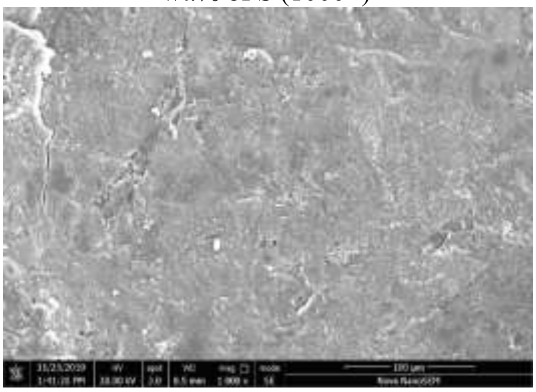

(e) Microstructures of the hydration products on the fracture surface of new concrete with 0.5 wt.% of MLG (1000×)

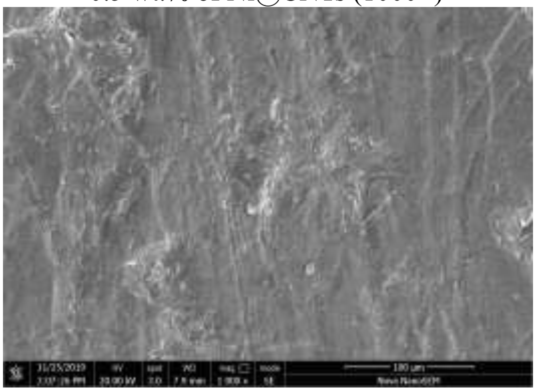

(f) Microstructures of the hydration products on the fracture surface of new concrete with 0.5 wt.% of NB (1000×)

Figure 7. Microstructures of the hydration products on the fracture surface of new concrete without/with nanoinclusions

Figure 8 shows the morphology of the calcium silicate hydrates (C-S-H) gels on the fracture surfaces of old concrete. A lot of micropores are found on the old concrete fracture surface of the specimens without nanoinclusions. Conversely, the addition of nanoinclusions allows the hydration products of nanoinclusions reinforced concrete to fill into the micropores of the old concrete, therefore, no obvious micropores are observed on the fracture surfaces of old concrete.

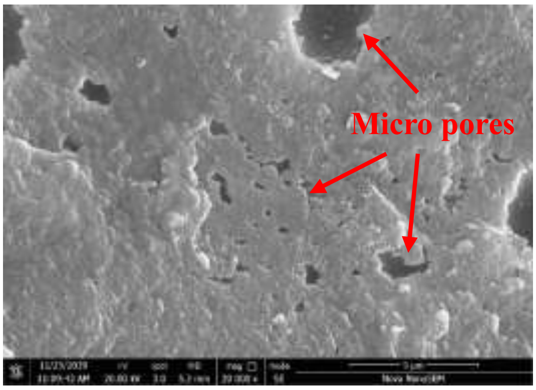

(a) C-S-H gel microstructure on the old concrete fracture surface of specimens without nanoinclusions (20000×)

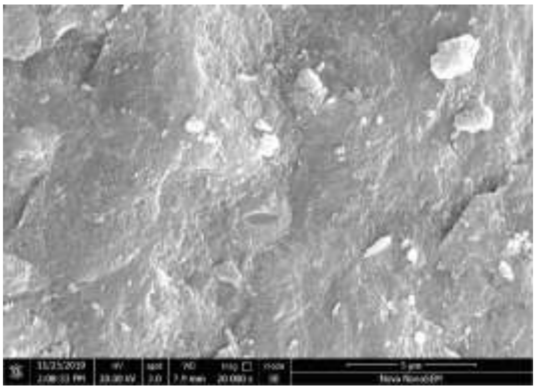
(b) C-S-H gel microstructure on the old concrete fracture surface of specimens with 3 wt.% of T (20000×)

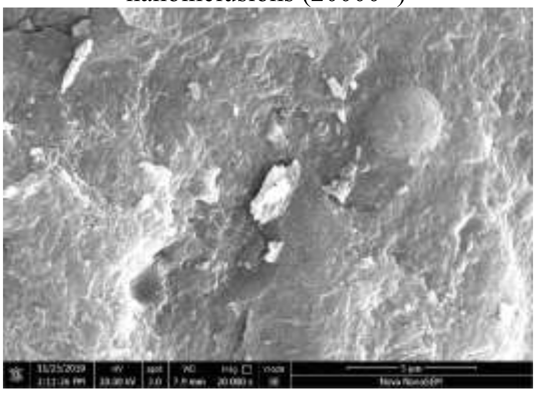
(c) C-S-H gel microstructure on the old concrete fracture surface of specimens with 1 wt.% of S (20000×)

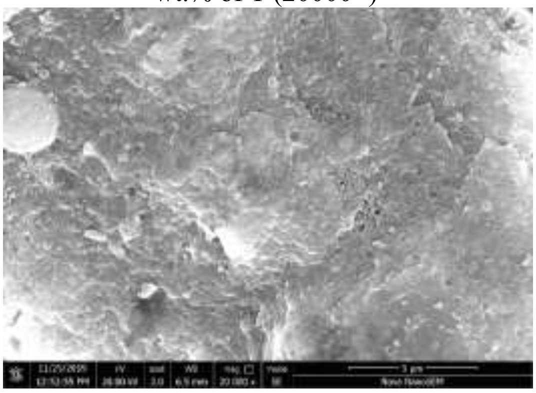
(d) C-S-H gel microstructure on the old concrete fracture surface of specimens with 0.5 wt.% of Ni@CNTs (20000×)

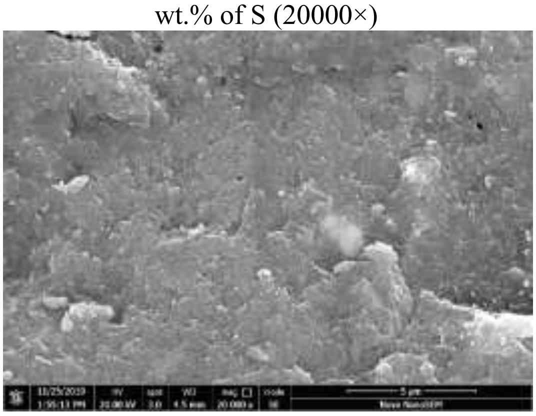
(e) C-S-H gel microstructure on the old concrete fracture surface of specimens with 0.5 wt.% of MLG (20000×)

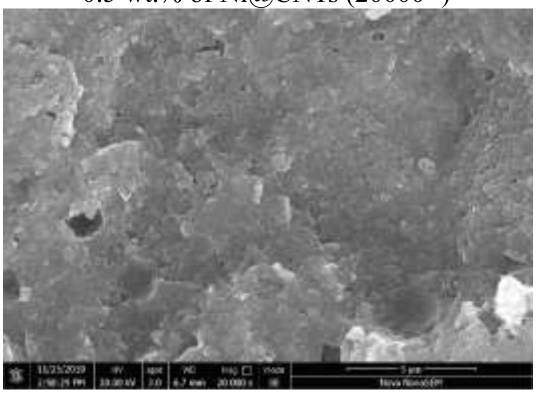
(f) C-S-H gel microstructure on the old concrete fracture surface of specimens with 0.5 wt.% of NB (20000×)

Figure 8. The microstructures of C-S-H gel on old concrete surface

Figure 9 illustrates the morphology of C-S-H gels on the fracture surface of new concrete with nanoinclusions. The C-S-H gels on the fracture surface of concrete without nanoinclusions are loose and porous, containing a lot of CH crystals. Besides, the average molar ratio of CaO to SiO_2 (Ca/Si ratio) of the C-S-H gel on the surface of concrete without nanoinclusions is 0.70, as listed in Table 3. On the contrary, the presence of nanoinclusions makes the C-S-H gels more uniform and improves the compactness, meanwhile, the Ca/Si ratio of C-S-H gels increases to 0.84-1.02 except for the incorporation of S. Meanwhile, the Ca/Si ratio of C-S-H gels on the fracture surface of new concrete with 1 wt.% of S reduces to 0.59, which may be caused by the enrichment of S in the new-to-old concrete interface.

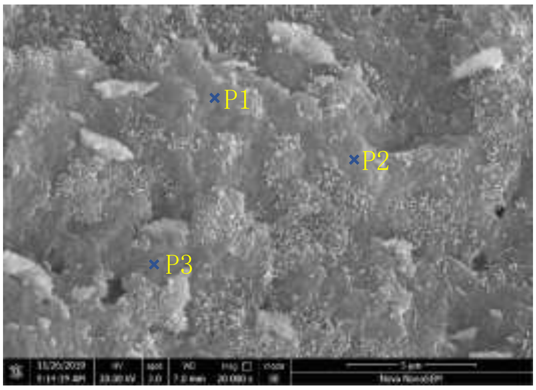

(a) C-S-H gel microstructure on the fracture surface of new concrete without nanoinclusions (20000×)

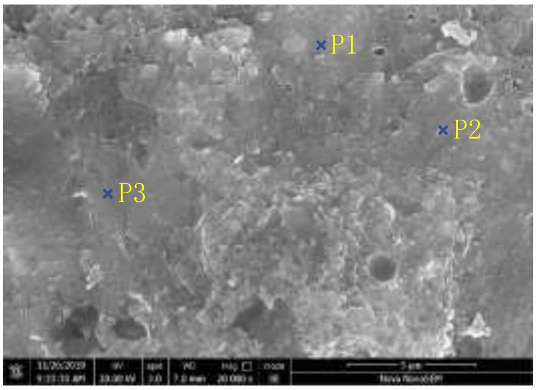

(b) C-S-H gel microstructure on the fracture surface of new concrete with 3 wt.% of T (20000×)

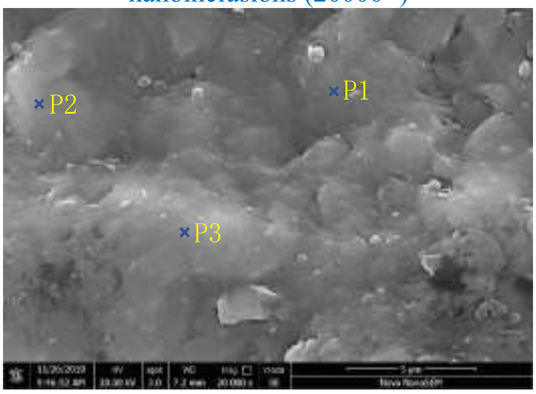

(c) C-S-H gel microstructure on the fracture surface of new concrete with 1 wt.% of S (20000×)

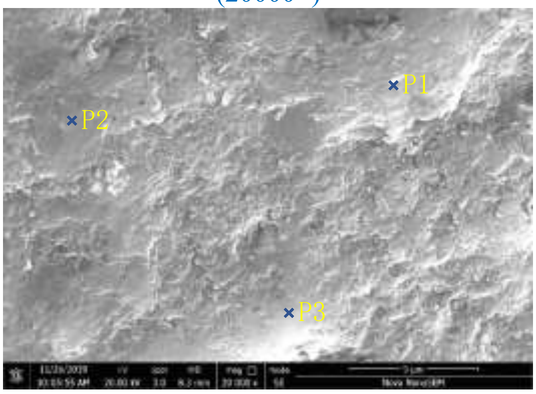

(d) C-S-H gel microstructure on the fracture surface of new concrete with 0.5 wt.% of Ni@CNTs (20000×)

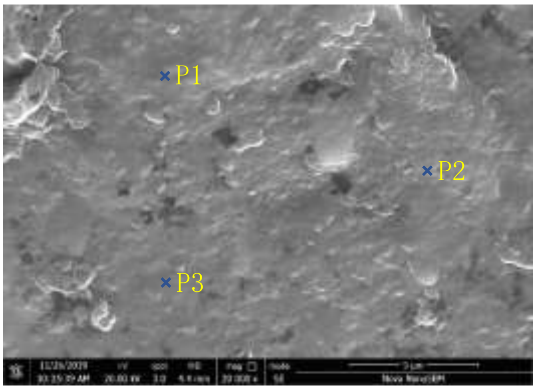

(e) C-S-H gel microstructure on the fracture surface of new concrete with 0.5 wt.% of MLG (20000×)

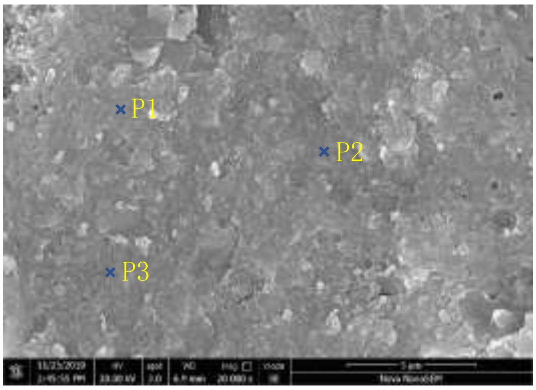

(f) C-S-H gel microstructure on the fracture surface of new concrete with 0.5 wt.% of NB (20000×)

Figure 9. C-S-H gel microstructure on the fracture surface of new concrete without/with nanoinclusions

Table 3. Ca/Si ratio of C-S-H gel on the fracture surface of new concrete with nanoinclusions

Code	EDS analysis point*	Ca (Atomic %)	Si (Atomic %)	Ca/Si ratio	Average Ca/Si ratio
Blank	P1	13.98	18.13	0.77	0.72
	P2	14.89	20.80	0.71	
	P3	14.31	21.24	0.67	
T-3	P1	13.94	20.09	0.69	0.84
	P2	14.88	15.73	0.95	
	P3	14.22	16.37	0.87	
S-1	P1	12.98	21.05	0.62	0.59
	P2	14.88	25.62	0.58	
	P3	9.83	17.59	0.56	
Ni@CNTs-0.5	P1	18.02	16.47	1.09	1.02
	P2	12.51	13.98	0.89	
	P3	20.72	19.52	1.06	
MLG-0.5	P1	21.53	21.37	1.01	1.02
	P2	25.08	22.89	1.10	
	P3	18.19	18.86	0.96	
NB-0.5	P1	15.26	14.44	1.06	0.98
	P2	11.86	12.12	0.98	
	P3	14.7	16.08	0.91	

* The EDS analysis point refers to the markings in Figure 9.

The bond strength of new-to-old concrete interface depends on the combination of chemical bonding (namely ionic bonding and covalent bonding), physical bonding (related to the van der Waals and surface tension forces), and mechanical interlock (concerned with interpenetration of concrete into roughness and porosity of old concrete) [1, 40, 41]. However, the chemical bonding in new-to-old concrete is so weak that can be ignored. As aforementioned, a nanoinclusion enrichment layer forms in the new-to-old concrete interface, which can notably improve the physical bonding and mechanical interlock between new and old concrete.

The nanoinclusions can notably improve the physical bonding between nanoinclusions reinforced concrete and old concrete. Previous studies reported that nanoinclusions in concrete can form numerous nano-core-shell structures during the hydration process [42-44]. Therefore, the aforementioned nanoinclusion enrichment layer can provide a large number of nucleation sites near the old concrete surface, thereby compacting the microstructures and further enhancing the physical bonding of new-to-old concrete interface. The reinforcing effect of the physical bonding between nanoinclusions reinforced concrete and old concrete is shown in Figure 10.

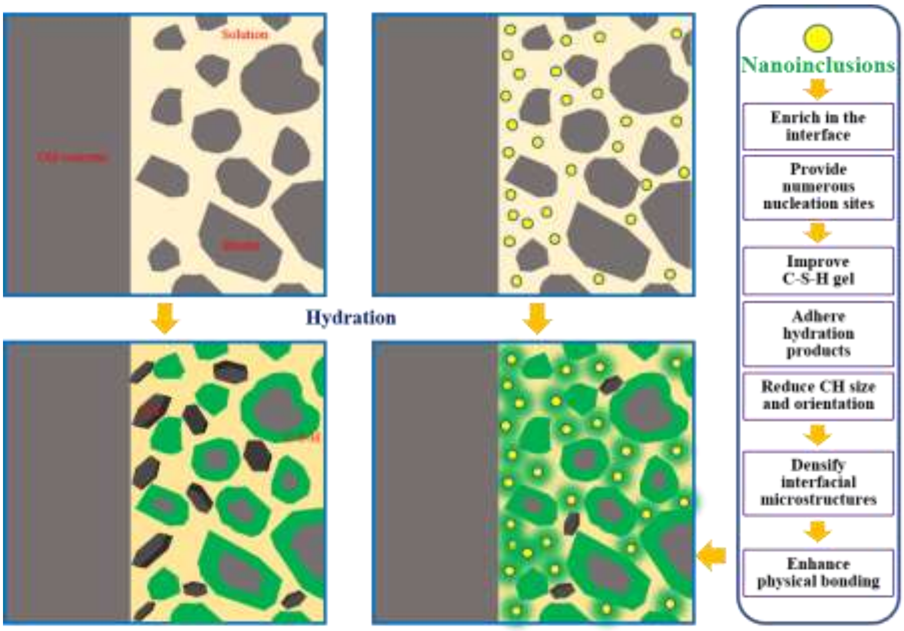

Figure 10. The enhancing effect of physical bonding between nanoinclusions reinforced concrete and old concrete

The nanoinclusions also have a strong effect on the mechanical interlock between nanoinclusions reinforced concrete and old concrete. For the polished old concrete surface, the mechanical interlock is weak because the roughness is low and the binder particles with the average particle size of 30 μm cannot be hydrated in capillary pores with the pore diameter of tens of nanometers [45]. In contrast, as shown in Figure 11, the nanoinclusions migrate into the micropores of the old concrete with water and provide nucleation sites at the early stage, allowing hydration products in micropores connect with that in bulk new concrete, thus enhancing the mechanical interlock between nanoinclusions reinforced concrete and old concrete.

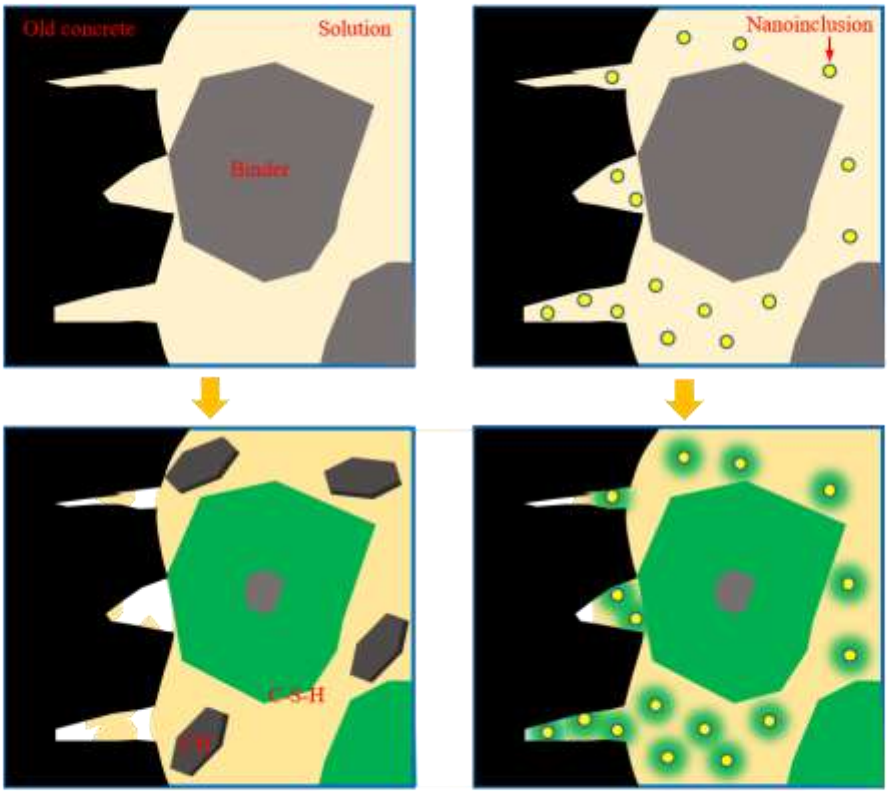

Figure 11. The enhancing effect of mechanical interlock between nanoinclusions reinforced concrete and old concrete

3.3 Prediction model of bond strength

Based on the previous analysis, the bond strength between nanoinclusions reinforced concrete and old strength is higher than that between new concrete without nanoinclusions and old concrete due to the enhancement of physical bonding and mechanical interlock. The physical bonding, mainly van der Waals forces, is affected by the microstructures of concrete. Therefore, this enhancement is based on the effect of nanoinclusions on the microstructures of concrete, represented by the splitting tensile strength of nanoinclusions reinforced concrete. The splitting tensile strength of nanoinclusions reinforced concrete can be predicted by Equation (3).

$$f_{tn} = f_t(1 + \alpha V) \quad (3)$$

where f_{tn} is the splitting tensile strength of nanoinclusions reinforced concrete, f_t is the splitting tensile strength of concrete without nanoinclusions, V represents the volume content of nanoinclusions in the concrete, α is the nanoinclusion enhancement coefficient, which can be fitted by experimental results. The fitting results of the splitting strength of nanoinclusions reinforced concrete are illustrated in Figure 12 and Table 4. It can be seen that the fitting degree of the relation between nanoinclusion volume content and splitting tensile strength of nanoinclusions reinforced concrete is high; the goodness of fit (R^2) ranges from 0.839-0.9936. Based on the fitting results, it can be deduced that the enhancement effect of nanoinclusions on the splitting tensile strength of concrete can be generally reflected by the geometrical size, i.e. nanosheets > nanotubes > nanoparticles.

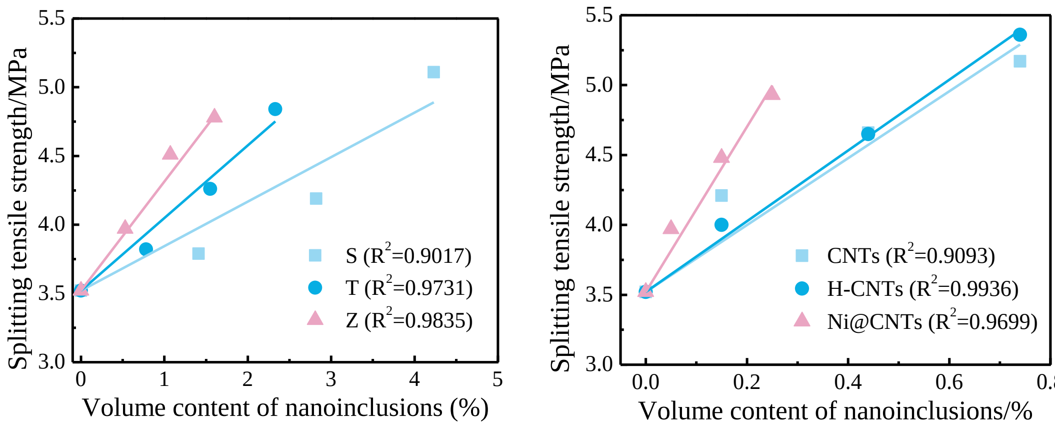

(a) Fitting results of splitting tensile strength of concrete with nanoparticles

(b) Fitting results of splitting tensile strength of concrete with nanotubes

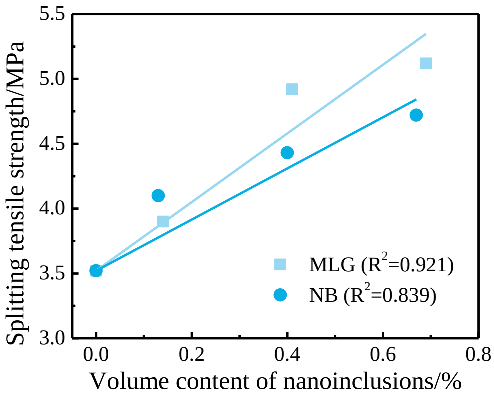

(c) Fitting results of splitting tensile strength of concrete with nanosheets

Figure 12. Fitting results of splitting tensile strength of concrete with nanoinclusions

In addition, the enhancement of bond strength of nanoinclusions reinforced concrete and old strength is also attributed to the mechanical interlock. As aforementioned, the nanoinclusions can enter the micropores on the old concrete surface and provide nucleation sites, thus increasing the mechanical interlock between nanoinclusions reinforced concrete and old concrete. It can be deduced that this enhancement is highly related to the viscosity of fresh concrete with nanoinclusions, highly consistent with the previous research results [8, 46]. The content of nanoinclusions in the micropores of the old concrete surface is determined by the total flow of the solution migrating into the micropores. For fresh concrete, the liquid flow rate Q in the micropores can be written as Equation (4) [47].

$$Q = -\left(\frac{1}{8\eta}\int_0^{\infty} r_i^2 \Omega_i dr_i\right)\frac{dP}{dx} \tag{4}$$

where η is fluid viscosity; $r_i^2\Omega_i$ is the intrinsic properties of micropores on the old concrete surface, in which r_i is pore radius and Ω_i is the average area distribution function of pore i exposed on any arbitrary face cut perpendicular to the flow; dP/dx is fluid pressure gradient. Therefore, the ratio of liquid flow of fresh concrete with nanoinclusions to that without nanoinclusions can be calculated from Equation (5).

$$\frac{Q_n}{Q_0}=\frac{-\left(\frac{1}{8\eta_n}\int_0^{\infty} r_i^2\Omega_i dr_i\right)\frac{dP}{dx}}{-\left(\frac{1}{8\eta_0}\int_0^{\infty} r_i^2\Omega_i dr_i\right)\frac{dP}{dx}}=\frac{\eta_0}{\eta_1}=\frac{1}{\eta_r} \tag{5}$$

where Q_n and Q_0 is the liquid flow rate of fresh concrete with and without nanoinclusions, respectively; η_n and η_0 is the plastic viscosity of fresh concrete with and without nanoinclusions, respectively; η_r is the relative plastic viscosity. According to reference [48-51], the plastic viscosity of fresh concrete can be predicted based on the cell method, as Equations (6)-(10).

$$\eta_r = 1+\eta_i\lambda \tag{6}$$

$$\lambda = y^3\frac{4(1-y^7)}{4(1+y^{10})-25y^3(1+y^4)+42y^5} \tag{7}$$

$$y=(\varphi/\varphi_{max})^{1/3}(1-K) \tag{8}$$

$$K = 3.8\cdot\frac{V_{sp}}{V_c}\cdot\frac{V_w}{V_s} \tag{9}$$

$$\varphi_{max} = 1-0.45\cdot\left(\frac{D_{10}}{D_{90}}\right)^{0.19} \tag{10}$$

where η_i is the intrinsic viscosity; φ is the volume concentration of solid particles in fresh concrete, φ_{max} is the maximum packing density; V_{sp}, V_c, V_w, V_s is the volume concentration of superplasticizer, cement, water, solid particle in fresh concrete, respectively; D_{10} and D_{90} is the sieve sizes corresponding to 10% and 90%, respectively.

As for the prediction of the bond strength of nanoinclusions reinforced concrete and old concrete, the bond strength can be written as in Equation (11).

$$f_b = \beta f_{to} \tag{11}$$

where f_b is the new-to-old concrete bond strength; β is the interfacial strength coefficient that equals to the ratio of the bond strength to the splitting tensile strength of old concrete; f_{to} is the splitting tensile strength of old concrete. The incorporation of nanoinclusions can enlarge the interfacial strength coefficient by compacting the microstructures, but undermine it due to the liquidity loss of fresh concrete. Therefore, the interfacial bond strength coefficient of nanoinclusions reinforced concrete and old concrete can be written as Equation (12).

$$\beta_n = \beta_0 \left(1 + \frac{\alpha\phi}{\eta_r} V\right) \tag{12}$$

where β_n is the interfacial strength coefficient of nanoinclusions reinforced concrete with old concrete; β_0 is the interfacial strength coefficient of new concrete without nanoinclusions with old concrete; ϕ is the nanoinclusion enrichment coefficient. In this experiment, superplasticizer is used as the dispersant of nanoinclusions, therefore part of superplasticizer is adsorbed by nanoinclusions, which reduces the plastic viscosity of fresh concrete. Therefore, the effective volume concentration of superplasticizer $V_{sp,eff}$ can be written as in Equation (13).

$$V_{sp,eff} = V_{sp} \cdot (1 - \gamma V) \tag{13}$$

where γ is the weakening coefficient of nanoinclusions to superplasticizer. Combining Formula (6)-(13) and experimental results, the γ can be fitted, as shown in Figure 13 and Table 4. It can be seen that the fitting degree of the relation between nanoinclusion volume content and bond strength of nanoinclusions reinforced concrete with old concrete is high; the R^2 ranges from 0.8438-0.9963. In addition, the fitted nanoinclusion enrichment coefficients of T, Z, and NB is highly consistent with the experimental results in this study. Based on the fitting results, it can be concluded that the proposed prediction model can accurately describe the relationship of the nanoinclusion content and the bond strength of nanoinclusions reinforced concrete with old concrete.

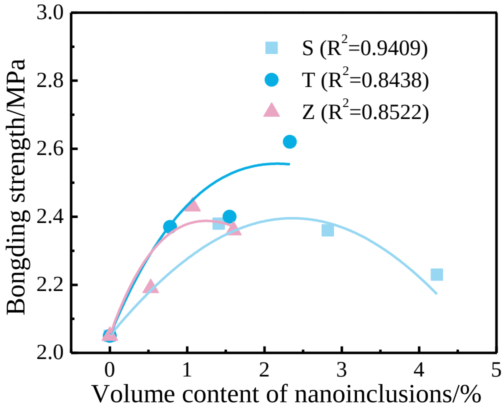

(a) Fitting results of bond strength of nanoparticles reinforced concrete with old concretes

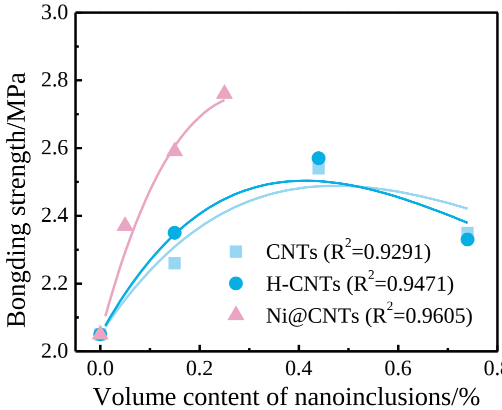

(b) Fitting results of bond strength of nanotubes reinforced concrete with old concrete

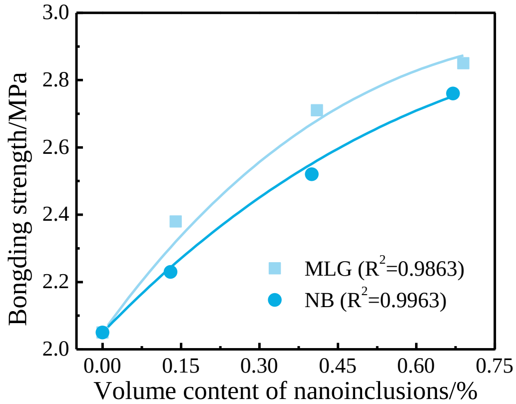

(c) Fitting results of bond strength of nanosheets reinforced concrete with old concrete

Figure 13. Fitting results of bond strength of nanoinclusions reinforced concrete with old concrete

Table 4. Fitting parameters of bond strength of nanoinclusions reinforced concrete with old concrete

Nanoinclusion	Nanoinclusion enhancement coefficient α	Nanoinclusion enrichment coefficient ϕ	Weakening coefficient γ
S	9.188	1.8	14.3162
T	15.029	2.0	37.4400
Z	22.577	1.4	58.3822
CNTs	67.962	1.6	160.8399
H-CNTs	71.866	1.8	177.2741
Ni@CNTs	167.96	1.6	234.8379
MLG	75.232	1.4	74.2485
NB	56.067	1.4	56.6331

4 Conclusions

The bond strength and its reinforcing mechanisms and prediction model of nanoinclusions reinforced concrete with old concrete have been investigated in this study. The following conclusions can be drawn:

- The bond strength between nanoinclusions reinforced concrete and old concrete is higher than that between new concrete without nanoinclusions and old concrete.
- The mechanisms for bond strength enhancement of nanoinclusions reinforced concrete with old concrete can be attributed to the improvement of the interfacial microstructures owing to the enriched presence of nanoinclusions in the new-to-old concrete interface. The enriched nanoinclusions can modify the compactness of the hydration products in the interface. The compact microstructures contribute to enhance the van der Waals forces between nanoinclusions reinforced concrete and old concrete as well as allow hydration products in micropores with that in bulk new concrete, thus enhancing the mechanical interlock between nanoinclusions reinforced concrete and old concrete.
- The proposed prediction model can accurately describe the relationship of the nanoinclusion content and the bond strength between nanoinclusions reinforced concrete and old concrete. This model can be used to guide the application of nanoinclusions reinforced concrete in the field of concrete repair.

In summary, this study demonstrates that the nanoinclusions reinforced concrete is a promising material for concrete rehabilitation and strengthening due to its reliable bonding with old concrete. Moreover, the mechanisms and model proposed in this paper provide references for further research and a basis for controlling the repair effects of nanoinclusions reinforced concrete.

Compliance with Ethical Standards

Funding: This study was funded by the National Science Foundation of China (51978127 and 51908103) and the China Postdoctoral Science Foundation

(2019M651116).
Conflict of Interest: The authors declare that they have no conflict of interest.

References

[1] Tayeh BA, Abu Bakar BH, Megat Johari MA, Zeyad AM. Microstructural analysis of the adhesion mechanism between old concrete substrate and UHPFC. J Adhes Sci Technol 2014; 28(18): 1846-1864.

[2] Espeche AD, León J. Estimation of bond strength envelopes for old-to-new concrete interfaces based on a cylinder splitting test. Constr Build Mater 2011; 25: 1222-1235.

[3] Khatib JM, Wright L, Mangat PS. Effect of desulphurised waste on long-term porosity and pore structure of blended cement pastes. Sustain Environ Res 2016; 26(5):230-234.

[4] Santos PMD, Julio ENBS. Factors affecting bond between new and old concrete. ACI Mater J 2011; 108(4): 449.

[5] Santos DS, Santos PM, Dias-da-Costa D. Effect of surface preparation and bonding agent on the concrete-to-concrete interface strength. Const Build Mater 2012; 37:102-110.

[6] He Y, Zhang X, Hooton RD, Zhang X. Effects of interface roughness and interface adhesion on new-to-old concrete bonding. Const Build Mater 2017; 151: 582-590.

[7] Santos PM, Julio EN. Correlation between concrete-to-concrete bond strength and the roughness of the substrate surface. Const Build Mater 2007; 21(8): 1688-1695.

[8] Tayeh BA, Bakar BA, Johari MM, Ratnam MM. The relationship between substrate roughness parameters and bond strength of ultra high-performance fiber concrete. J Adhes Sci Technol 2013; 27(16): 1790-1810.

[9] Chen PW, Fu X, Chung DDL. Improving the bonding between old and new concrete

by adding carbon fibers to the new concrete. Cement Concrete Res 1995; 25(3): 491-496.

[10] Sun W, Sebastian W, Keller T, Ross J. Mixed mode fracture properties of GFRP-adhesive interfaces based on video gauge and acoustic emission measurements from specimens with adherend fibres normal to the interfaces. Compos Part B-Eng 2017; 123: 179-192.

[11] Li GY, Xie HC, Xiong GJ. Transition zone studies of new-to-old concrete with different binders. Cement Concrete Comp 2001; 23(4-5): 381-387.

[12] Ardalan RB, Joshaghani A, Hooton RD. Workability retention and compressive strength of self-compacting concrete incorporating pumice powder and silica fume. Const Build Mater 2017; 134:116-122.

[13] Noorvand H, Ali AAA, Demirboga R, Farzadnia N, Noorvand H. Incorporation of nano TiO_2 in black rice husk ash mortars. Const Build Mater 2013; 47: 1350-1361.

[14] Khaloo A, Mobini MH, Hosseini P. Influence of different types of nano-SiO_2 particles on properties of high-performance concrete. Const Build Mater 2016; 113: 188-201.

[15] Li GY, Wang PM, Zhao XH. Mechanical behavior and microstructure of cement composites incorporating surface-treated multi-walled carbon nanotubes. Carbon 2005; 43(6): 1239-1245.

[16] Joshaghani A, Balapour M, Mashhadian M, Ozbakkaloglu T. Effects of nano-TiO_2, nano-Al_2O_3, and nano-Fe_2O_3 on rheology, mechanical and durability properties of self-consolidating concrete (SCC): An experimental study. Const Build Mater 2020; 245: 118444.

[17] Mullapudi R, Ayoub, A. Analysis of concrete structures reinforced with carbon nano-fibers. In: IABSE Symposium Report, International Association for Bridge and

Structural Engineering 2012 98; 3: 42-49.

[18] Hawreen A, Bogas JA. Creep, shrinkage and mechanical properties of concrete reinforced with different types of carbon nanotubes. Const Build Mater 2019; 198: 70-81.

[19] Miyandehi BM, Feizbakhsh A, Yazdi MA, Liu QF, Yang, J, Alipour P. Performance and properties of mortar mixed with nano-CuO and rice husk ash. Cement Concrete Comp 2016; 74:225-235.

[20] Szymanowski J, Sadowski Ł. The influence of the addition of tetragonal crystalline titanium oxide nanoparticles on the adhesive and functional properties of layered cementitious composites. Compos Struct 2020; 233: 111636.

[21] Szymanowski J, Sadowski Ł. The development of nanoalumina-based cement mortars for overlay applications in concrete floors. Materials 2019: 12(21); 3465.

[22] Manzur T, Yazdani N, Emon M, Bashar A. Potential of carbon nanotube reinforced cement composites as concrete repair material. Journal of Nanomaterials 2016.

[23] Haruehansapong S, Pulngern T, Chucheepsakul S. Effect of nanosilica particle size on the water permeability, abrasion resistance, drying shrinkage, and repair work properties of cement mortar containing nano-SiO_2. Adv Mater Sci Eng, 2017.

[24] Yıldırım G, Dündar B, Alam B, Şahmaran M. Role of nanosilica on the early-age performance of natural pozzolan-based blended cement. ACI Mater J 2018; 115(6).

[25] Szymanowski J, Sadowski Ł. Functional and adhesive properties of cement-based overlays modified with amorphous silica nanospheres. J Adhesion 2019; 1-22.

[26] Anike EE, Saidani M, Ganjian E, Tyrer M, Olubanwo AO. The potency of recycled aggregate in new concrete: a review. Constr Innov 2019.

[27] Nazari A, Riahi S. The effects of zinc dioxide nanoparticles on flexural strength of self-compacting concrete. Compos Part B-Eng 2011; 42(2): 167-175.

[28] Zhang LQ, Ma N, Wang YY, Han BG, Cui X, Yu X, Ou JP. Study on the reinforcing mechanisms of nano silica to cement-based materials with theoretical calculation and experimental evidence. J Compos Mater 2016; 50(29): 4135-4146.

[29] Funk JE, Dinger DR. Predictive process control of crowded particulate suspensions: applied to ceramic manufacturing. Burlin: Springer, 2013.

[30] Brouwers HJH. Particle-size distribution and packing fraction of geometric random packings. Phys Rev E 2006; 74(3): 031309.

[31] Yu R, Spiesz P, Brouwers HJH. Mix design and properties assessment of ultra-high performance fibre reinforced concrete (UHPFRC). Cement Concrete Res 2014; 56: 29-39.

[32] Yu R, Song Q, Wang X, Zhang Z, Shui Z, Brouwers HJH. Sustainable development of Ultra-High Performance Fibre Reinforced Concrete (UHPFRC): Towards to an optimized concrete matrix and efficient fibre application. J Clean Prod 2017; 162: 220-233.

[33] Wang XY, Dong SF, Ashour A, Zhang W, Han BG. Effect and mechanisms of nanomaterials on interface between aggregates and cement mortars. Const Build Mater 2020; 240: 117942.

[34] Wang ZX, Yu QL, Gauvin F, Feng P, Ran QP, Brouwers HJH. Nanodispersed TiO_2 hydrosol modified Portland cement paste: The underlying role of hydration on self-cleaning mechanisms. Cement Concrete Res 2020; 136: 106156.

[35] Liu X, Feng P, Shu X, Ran QP. Effects of highly dispersed nano-SiO_2 on the microstructure development of cement pastes. Mater design 2020; 53: 4.

[36] Han B, Li Z, Zhang L, Zeng S, Yu X, Han B, Ou J. Reactive powder concrete reinforced with nano SiO_2-coated TiO_2. Const Build Mater 2017; 148: 104-112.

[37] Cui X, Han BG, Zheng QF, Yu X, Dong SF, Zhang LQ, Ou JP. Mechanical

properties and reinforcing mechanisms of cementitious composites with different types of multiwalled carbon nanotubes. Compos Part A-Appl S 2017; 103: 131-147.

[38] Chinese National Standard. Standard for test methods of concrete physical and mechanical properties, GB/T 50081-2019. Beijing, 2019.

[39] Forsyth DA, Ponce J, Computer Vision A Modern Approach, New York: Pearson, 2012.

[40] Austin S, Robins P, Pan Y. Tensile bond testing of concrete repairs. Mater Struct 1995; 28(5): 249.

[41] Bissonnette B, Nuta A, Morency M, Marchand J, Vaysburd A. Concrete repair and interfacial bond: Influence of surface preparation. In: Concrete Repair, Rehabilitation and Retrofitting II: 2nd International Conference on Concrete Repair, Rehabilitation and Retrofitting, Cape Town, South Africa, 2008

[42] Wang XY, Zheng QF, Dong SF, Ashour A, Han BG. Interfacial characteristics of nano-engineered concrete composites. Const Build Mater 2020; 259: 119803.

[43] Han BG, Zhang LQ, Zeng SZ, Dong SF, Yu X, Yang RF, Ou JP. Nano-core effect in nano-engineered cementitious composites. Compos Part A-Appl S 2017; 95: 100-109.

[44] Han BG, Ding SQ, Wang JL, Ou JP. Nano-Engineered Cementitious Composites: Principles and Practices. Burlin: Springer, 2019.

[45] Bijen J, Salet T. Adherence of young concrete to old concrete development of tools for engineering. In: Proceedings of the 2nd Bolomey Workshop, 1993.

[46] Courard L, Piotrowski T, Garbacz A. Near-to-surface properties affecting bond strength in concrete repair. Cement Concrete Comp 2014; 46: 73-80.

[47] Song HW, Kwon SJ. Permeability characteristics of carbonated concrete considering capillary pore structure. Cement Concrete Res 2007; 37(6): 909-915.

[48] Mahmoodzadeh F, Chidiac SE. Rheological models for predicting plastic viscosity and yield stress of fresh concrete. Cement Concrete Res 2013; 49: 1-9.

[49] Hu C, de Larrard F. The rheology of fresh high-performance concrete. Cement Concrete Res 1996; 26(2): 283-294.

[50] Krieger IM, Dougherty TJ. A mechanism for non-Newtonian flow in suspensions of rigid spheres. Trans Soc Rheolo 1959; 3(1): 137-152.

[51] Chidiac SE, Mahmoodzadeh F. Plastic viscosity of fresh concrete-A critical review of predictions methods. Cement Concrete Compos 2009; 31(8): 535-544.